

RESEARCH ARTICLE

Longitudinal neural connection detection using a ferritin-encoding adeno-associated virus vector and in vivo MRI method

Aoling Cai^{1,2} | Ning Zheng² | Garth J. Thompson³ | Yang Wu^{2,4} | Binbin Nie⁵ | Kunzhang Lin⁶ | Peng Su⁶ | Jinfeng Wu² | Anne Manyande⁷ | LingQiang Zhu⁸ | Jie Wang^{2,4,9}  | Fuqiang Xu^{1,2,4,6,10}

¹Wuhan National Laboratory for Optoelectronics, Huazhong University of Science and Technology, Wuhan, China

²Key Laboratory of Magnetic Resonance in Biological Systems, State Key Laboratory of Magnetic Resonance and Atomic and Molecular Physics, National Center for Magnetic Resonance in Wuhan, Wuhan Institute of Physics and Mathematics, Innovation Academy for Precision Measurement Science and Technology, Chinese Academy of Sciences-Wuhan National Laboratory for Optoelectronics, Wuhan, China

³Human Institute, ShanghaiTech University, Shanghai, China

⁴University of Chinese Academy of Sciences, Beijing, China

⁵Key Laboratory of Nuclear Radiation and Nuclear Energy Technology, Institute of High Energy Physics, Chinese Academy of Sciences, Beijing, China

⁶Shenzhen Key Lab of Neuropsychiatric Modulation, Guangdong Provincial Key Laboratory of Brain Connectome and Behavior, CAS Key Laboratory of Brain Connectome and Manipulation, the Brain Cognition and Brain Disease Institute (BCBDI), Shenzhen Institutes of Advanced Technology, Chinese Academy of Sciences; Shenzhen-Hong Kong Institute of Brain Science-Shenzhen Fundamental Research Institutions, Shenzhen, China

⁷School of Human and Social Sciences, University of West London, London, UK

⁸Department of Pathophysiology, Key Lab of Neurological Disorder of Education Ministry, School of Basic Medicine, Tongji Medical College, Huazhong University of Science and Technology, Wuhan, China

⁹Hebei Provincial Key Laboratory of Basic Medicine for Diabetes, 2nd Hospital of Shijiazhuang, Shijiazhuang, Hebei, China

¹⁰Center for Excellence in Brain Science and Intelligent Technology, Chinese Academy of Sciences, Shanghai, China

Correspondence

Jie Wang, Key Laboratory of Magnetic Resonance in Biological Systems, State Key Laboratory of Magnetic Resonance and Atomic and Molecular Physics, National Center for Magnetic Resonance in Wuhan, Wuhan Institute of Physics and Mathematics, Innovation Academy for Precision Measurement Science and Technology, Chinese Academy of Sciences-Wuhan National Laboratory for Optoelectronics, Wuhan 430071, China.
Email: jie.wang@wipm.ac.cn

Fuqiang Xu, Shenzhen Key Lab of Neuropsychiatric Modulation, Guangdong Provincial Key Laboratory of Brain Connectome and Behavior, CAS Key Laboratory of Brain Connectome and Manipulation, the Brain Cognition and Brain Disease Institute (BCBDI), Shenzhen Institutes

Abstract

The investigation of neural circuits is important for interpreting both healthy brain function and psychiatric disorders. Currently, the architecture of neural circuits is always investigated with fluorescent protein encoding neurotropic virus and ex vivo fluorescent imaging technology. However, it is difficult to obtain a whole-brain neural circuit connection in living animals, due to the limited fluorescent imaging depth. Herein, the noninvasive, whole-brain imaging technique of MRI and the hypotoxicity virus vector AAV (adeno-associated virus) were combined to investigate the whole-brain neural circuits in vivo. AAV2-retro are an artificially-evolved virus vector that permits access to the terminal of neurons and retrograde transport to their cell bodies. By expressing the ferritin protein which could accumulate iron ions and influence the MRI contrast, the neurotropic virus can cause MRI signal changes in the infected regions. For mice injected with the ferritin-encoding virus vector (rAAV2-retro-CAG-

Aoling Cai and Ning Zheng contributed equally to this work.

This is an open access article under the terms of the Creative Commons Attribution-NonCommercial-NoDerivs License, which permits use and distribution in any medium, provided the original work is properly cited, the use is non-commercial and no modifications or adaptations are made.

© 2021 Innovation Academy for Precision Measurement Science and Technology. *Human Brain Mapping* published by Wiley Periodicals LLC.

of Advanced Technology, Chinese Academy of Sciences; Shenzhen-Hong Kong Institute of Brain Science-Shenzhen Fundamental Research Institutions, Shenzhen 518055, China.

Email: fuqiang.xu@wipm.ac.cn

Funding information

National Natural Science Foundation of China, Grant/Award Numbers: 31771193, 31970973, 21921004; National Natural Science Foundation of Hubei Province, Grant/Award Number: 2020CFA059; the Open Project Program of Wuhan National Laboratory for Optoelectronics, Grant/Award Number: 2019WNLOKF022; the Strategic Priority Research Program of the Chinese Academy of Sciences, Grant/Award Number: XDB32030200; the Youth Innovation Promotion Association of Chinese Academy of Sciences, Grant/Award Number: Y6Y0021004; Key-Area Research and Development Program of Guangdong Province, Grant/Award Number: 2018B030331001

Ferritin) in the caudate putamen (CPU), several regions showed significant changes in MRI contrasts, such as PFC (prefrontal cortex), HIP (hippocampus), Ins (insular cortex) and BLA (basolateral amygdala). The expression of ferritin in those regions was also verified with *ex vivo* fluorescence imaging. In addition, we demonstrated that changes in T2 relaxation time could be used to identify the spread area of the virus in the brain over time. Thus, the neural connections could be longitudinally detected with the *in vivo* MRI method. This novel technique could be utilized to observe the viral infection process and detect the neural circuits in a living animal.

KEYWORDS

ferritin, immunohistochemistry, *in vivo* MRI, neural circuit, rAAV2-retro

1 | INTRODUCTION

The brain is the most complex organ in the body, and more than 70 billion neurons exist in the human brain to form a complicated network (Grandjean et al., 2020). More and more preclinical studies have shown that neural networks play an essential role in instinctive behaviors such as fear (Wei et al., 2015), reward (Zhang et al., 2017) and mating (Wei et al., 2018). In addition, the alteration of neural networks may lead to abnormal animal behaviors, such as epilepsy-like (Cittraro et al., 2013) or depression-like behaviors (Rozov, Jerecic, Sakmann, & Burnashev, 2001), suggesting that human brain diseases may emerge from neural network dysfunction. Dissecting neural networks is important for understanding brain function in a physiological or pathological state.

Currently, neurotropic viral vectors have been widely used to investigate the neural networks. As a series of artificially modified neurotropic viruses, neurotropic viral vectors can transport exogenous genes along the synapses-connected neural networks. Numerous virus vectors were constructed to dissect the structure of neural networks after genetic modifications, such as herpes simplex virus (HSV), pseudorabies virus (PRV), rabies virus (RV), etc. (Nassi, Cepko, Born, & Beier, 2015; Rao & Wang, 2020; Ugolini, 2010). However, most of them can only be used for *ex vivo* imaging due to their virulence. Recombinant adeno-associated virus (rAAV) vectors are effective tools for exogenous gene delivery for living animal studies due to their advantages of high-level transgene expression and low cell toxicity (Kaplit et al., 2007). Recently an artificially evolved AAV series vector (rAAV2-retro) was introduced to mediate retrograde access to neurons (Tervo et al., 2016). It is a powerful tool to image neural circuits when combined with the fluorescent protein gene (Zheng et al., 2020). However, due to limitation of the fluorescent imaging depth, it is hard to observe the whole-brain neural circuit in a living animal, which also impedes our understanding of the virus infection

procedures. Thus, it was valuable to develop a novel method for *in vivo* neuronal network detection.

A vast amount of impressive work has been done for living animal imaging. Near-infrared (NIR) fluorescence imaging methods have been used to increase the imaging depth of fluorescent protein (Frangioni, 2003) and allow for *in vivo* imaging (Hong, Antaris, & Dai, 2017). However, the NIR signal is only reliable within the depth of 3 mm (Hong et al., 2014). Luciferase has also been used as an *in vivo* imaging strategy because, with a highly sensitive detector, the imaging depth can be up to 40 mm. While this has been valuable for labeling cancer cells and gene expression (Li et al., 2017), the spatial resolution of luciferase imaging is not sufficient enough for tracing neural circuits (Cook & Griffin, 2003). Magnetic resonance imaging (MRI) is a commonly used clinical image technique, which has the advantages of non-invasive and large-scale imaging (Van Leemput et al., 2009; Wu, Wong, Andrassy, & Tang, 2003). The MRI also provides a good compromise of moderately high spatial resolution (~100 μm) while covering the entire brain (Pagani, Damiano, Galbusera, Tsaftaris, & Gozzi, 2016; Ullmann, Watson, Janke, Kurniawan, & Reutens, 2013). Thus, with a proper MRI contrast agent encoded by the virus vector, MRI could be an excellent tool to trace the whole-brain neural networks in living animals.

Ferritin is a ubiquitous iron storage protein found in most organisms. In general, it protects the cell from damaging active oxide Fe^{2+} and stores the iron ion in the shell of ferritin as Fe^{3+} . As Fe^{3+} is a paramagnetic MRI contrast agent, the overexpression of ferritin is able to change the transverse magnetic relaxation rate ($1/T_2$) of the surrounding tissue. Thus, at sufficiently high concentration and with sufficient access to biological iron, ferritin can change the contrast of the MRI signal and show its presence with hypointensity on T2-weighted MRI images (Iordanova & Ahrens, 2012; Wu et al., 2018). In our previous work, the ferritin gene was loaded onto the VSV (vesicular stomatitis virus) and a multi-synaptic neural network connected to sensory cortex was illustrated (Zheng et al., 2019).

However, the result was obtained using ex vivo MRI due to the virulence of the VSV. Here, we tried to display the whole-brain neural network in a living animal with hypotoxicity virus vector AAV.

Herein, a novel tool for in vivo whole-brain neural network imaging was developed. We loaded the ferritin gene onto a retrograde transporting AAV vector, delivered it to the caudate-putamen (CPu) of mice and imaged these mice with in vivo MRI. In doing so, we were able to visualize a CPu-connected network that includes the upstream brain regions sending projection to the CPu. The ferritin-encoding retrograde transporting AAV vector enabled the investigation of neural network in living animals and long-term observation of the virus infection.

2 | RESULTS

2.1 | MRI signal changes of the regions with ferritin transduction

First, the function of rAAV2-retro-CAG-Ferritin to label the neural networks and express ferritin was investigated. To this end, a control virus vector rAAV2-retro-CAG-EGFP was constructed for comparison (Figure 1a). These two virus vectors were injected into the CPu region of mice with similar titers (5×10^{12} vg/mL) and volumes (2.8 μ L). Sixty days after receiving the injection, the animals were firstly scanned with MRI and then sacrificed for slicing. The brain slices were performed immunohistochemical staining with anti-ferritin primary antibody and cy3 conjugated secondary antibody (red), and submitted to fluorescent imaging. The brain slices of these two groups with same stereotaxic coordinates were chosen for comparison (Figure 1b). Similar to the rAAV2-retro-CAG-EGFP infected group, the expression of ferritin could be found in multiple brain regions other than the injection site CPu, such as the PFC (prefrontal cortex), HIP (hippocampus), Ins (insular cortex), and BLA (basolateral amygdala). Most of those areas were directly connected to CPu (Tervo et al., 2016). Second, the MRI signals were also compared in the whole brain of mice infected with these two virus vectors. In rAAV2-retro-CAG-Ferritin infected group, the hypointensity MRI signals (compared to the surrounding tissue) were observed at ferritin expressed regions (Figure 1b, lower). Meanwhile, there was no discernible signal changes observed on the T2-weighted MRI image in the same regions with EGFP overexpression in the control group (Figure 1b, upper).

In order to dissect the neural circuit, the resolution and SNR (signal to noise ratio) of the MRI image should be sufficient enough to distinguish the structural regions or even the sub-regions of the brain. The fluorescence and MRI images of similar brain structures were expanded to illustrate the details of ferritin-encoding AAV expression (Figure 2). In the fluorescent images, the red fluorescent signals represented the expression of ferritin. In MRI images, the hypointensity MRI contrasts were regarded as the MRI contrast effect caused by ferritin expression and iron ions aggregation. Overlapping with a stereotaxic atlas of the mouse brain (Paxinos and Franklin), the location of ferritin could be plainly identified. Seven representative regions with obvious ferritin expression were collected for comparison, such

as CPu, BLA, HIP, PFC, Tha (Thalamus), Ins and posterior HIP (Figure 2b). Although the resolution and SNR of the MRI were much lower than fluorescence imaging, the same ferritin expressing regions could be detected by both MRI and fluorescence imaging. In addition, a more detailed brain partition atlas of the Ins region was used to explore whether subtle localized changes could be detected with in vivo MRI (Allen mouse brain atlas, <http://atlas.brain-map.org/>). Using this, MRI contrast changes caused by ferritin expression located in the fifth layer of the insular cortex, which is in line with the fluorescent imaging result. Thus, the subtle localized changes could also be detected using the MRI method.

2.2 | Long term observation of T2-weighted images with ferritin/EGFP expression

The longitudinal recording of rAAV2-retro-CAG-Ferritin and rAAV2-retro-CAG-EGFP infected groups were performed at different time points (0d, 10d, 30d, 60d) in the same animal using T2-weighted MRI (Figure S1). In consistent with the fluorescent images (Figure 2), several regions showed MRI contrasts changes at different time points, including PFC, BLA, Ins, and HIP. In the rAAV2-retro-CAG-Ferritin group, the changes in MRI contrast of those regions were discernable after 30 days' infection and became stronger at 60 days. Meanwhile, there were no significant changes observed in the rAAV2-retro-CAG-EGFP group during the whole period of infection.

To quantitatively measure changes in MRI contrast, six regions (CPu, PFC, BLA, Ins, HIP and Tha) with ferritin/EGFP expression were selected as ROIs (regions of interest) based on an open source MRI template (TMBTA), and the other two regions CSF (cerebrospinal fluid) and SC (superior colliculus) were chosen for comparison due to limited ferritin/EGFP expression (Figure S2). Signal intensity normalization (with CSF) were performed before statistical comparison, and the one-way ANOVA (LSD post hoc test) method was used to evaluate changes in signal intensity in the T2-weighted images following the infection days (Figure S3). In the rAAV2-retro-CAG-Ferritin infected group (0d, $N = 14$; 10d, $N = 11$; 30d, $N = 8$; 60d, $N = 5$), statistical differences in MRI contrast were observed in the virus infected regions following virus infection, such as CPu, BLA, HIP, PFC, Ins and Tha ($p < .05$), while no significant signal changes were detected in SC among different infection time points. Moreover, there were no significant MRI signal changes in all these brain regions of the rAAV2-retro-CAG-EGFP group during the entire virus infected periods (0d, $N = 3$; 10d, $N = 3$; 30d, $N = 3$; 60d, $N = 3$).

2.3 | Tracing CPu connected regions using changes in T2 relaxation time

To show the neural network in vivo with a whole-brain view, voxel-wise changes in T2 relaxation time were performed based on the normalized T2 relaxation time maps (Figure 3a). The multi-echo T2-weighted images

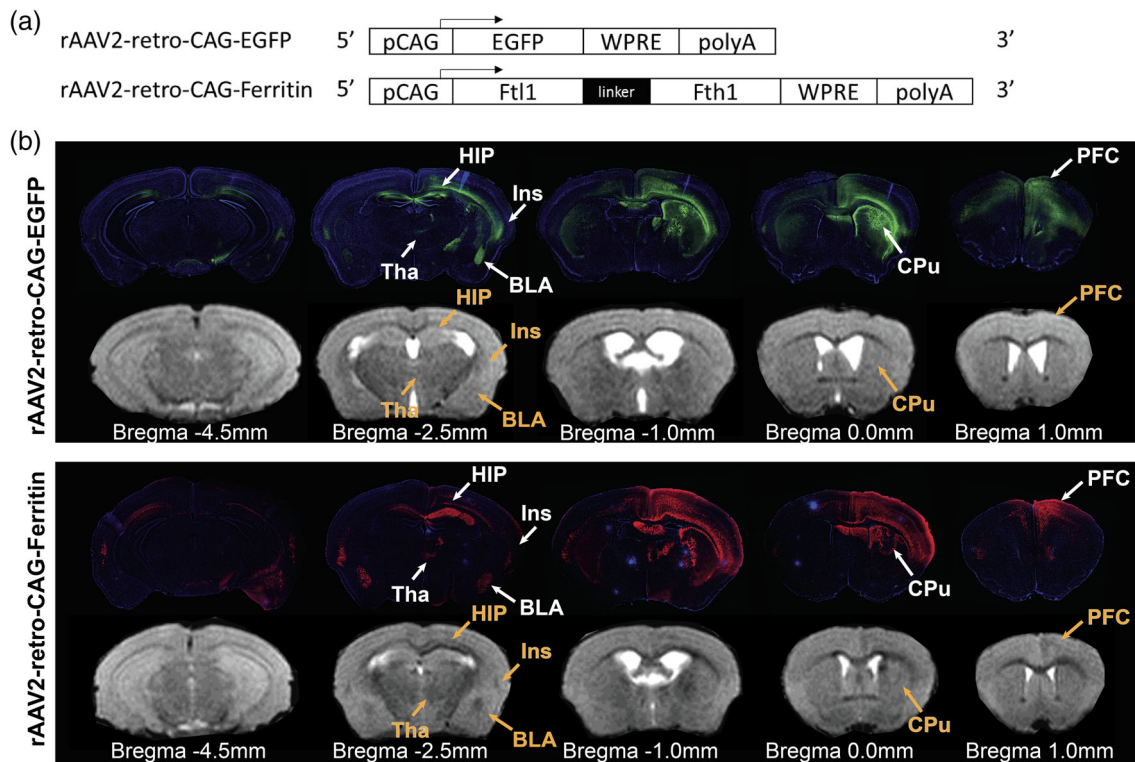


FIGURE 1 Detection of EGFP/ferritin expression with fluorescence imaging and T2-weighted MRI (TE = 55 ms), 60 days after the virus injection. (a) Virus genomes of rAAV2-retro-CAG-EGFP and rAAV2-retro-CAG-Ferritin, Ftl1: *Mus musculus* ferritin light chain, Fth1: *Mus musculus* ferritin heavy chain. (b) Upper, fluorescence images (green, EGFP) and corresponding MRI images (gray) of one representative mouse brain infected with rAAV2-retro-CAG-EGFP; lower, fluorescence images (red, ferritin) and corresponding MRI images (gray) of one representative mouse brain infected with rAAV2-retro-CAG-ferritin

were converted to T2 relaxation time maps and then normalized to a standard space base on the transformation matrix of T2-weighted images. The differences between T2 relaxation time maps before injection (0d, Figure 3b) and after injection (10d, 30d, 60d) were calculated voxel by voxel (Figure 3b) and then filtered by a threshold of 4–15 ms (Figure 4).

The mapping of T2 relaxation time changes was compared with fluorescent images and T2-weighted images with similar brain structures. The comparisons among three different time points were illustrated (Figure 4). Ten days after the injection, ferritin expression was observed in CPu and PFC with fluorescence imaging. The same regions were also detected in mapping of T2 relaxation time changes (10d), although the area was not as wide as the fluorescence imaging. Thirty days after infection, stronger signals were detected in PFC, CPu, Tha, BLA, HIP, and Ins from the fluorescence images, and wider signals were also found in PFC, CPu, BLA and Ins from the T2 relaxation time change mapping (30d). Sixty days after infection, the fluorescent signal spread across the whole-brain through the fluorescence imaging, particularly in the PFC, CPu, Tha, BLA, HIP and Ins. Consistently, the T2 relaxation time change mapping (60d) showed more similar labeled patterns compared to the fluorescence imaging. Overall, similar signal tendency was obtained from both the fluorescence imaging and the T2 relaxation time change mappings over the four infected periods. Thus, the changes in T2 relaxation time can be used to identify the spreading area of the virus in the brain over time.

Furthermore, the mapping of T2 relaxation time changes was utilized to investigate the CPu connected regions with the in vivo MRI approach in the same animal at different time points after the rAAV2-retro-CAG-Ferritin injection. The dynamic changes in MRI contrast were almost similar in all individual subjects (Figure 5). During the early stage of virus infection (10d), changes in T2 relaxation time was only observed at the injection site (CPu). Thirty days after the infection, more regions showed distinct changes in all the subjects, such as PFC, HIP and BLA. After 60 days, most of CPu single synapse connected regions were detected at the mapping of T2 relaxation time changes, such as PFC, BLA, Ins and Tha. Although the signals were unstable during the early stage of the infection, the changes in MRI contrast became stronger and more consistent after 60 days' infection. Thus, this method could be a promising way for investigating the neural circuits in living animals.

2.4 | Quantification of T2 relaxation time changes in ferritin transduction regions

The T2 relaxation time of ferritin overexpressed regions were further quantitatively measured to assess the MRI signal change along with the infection periods. Six regions with ferritin overexpression (CPu, BLA, HIP, Ins, PFC and Tha) and two regions without ferritin

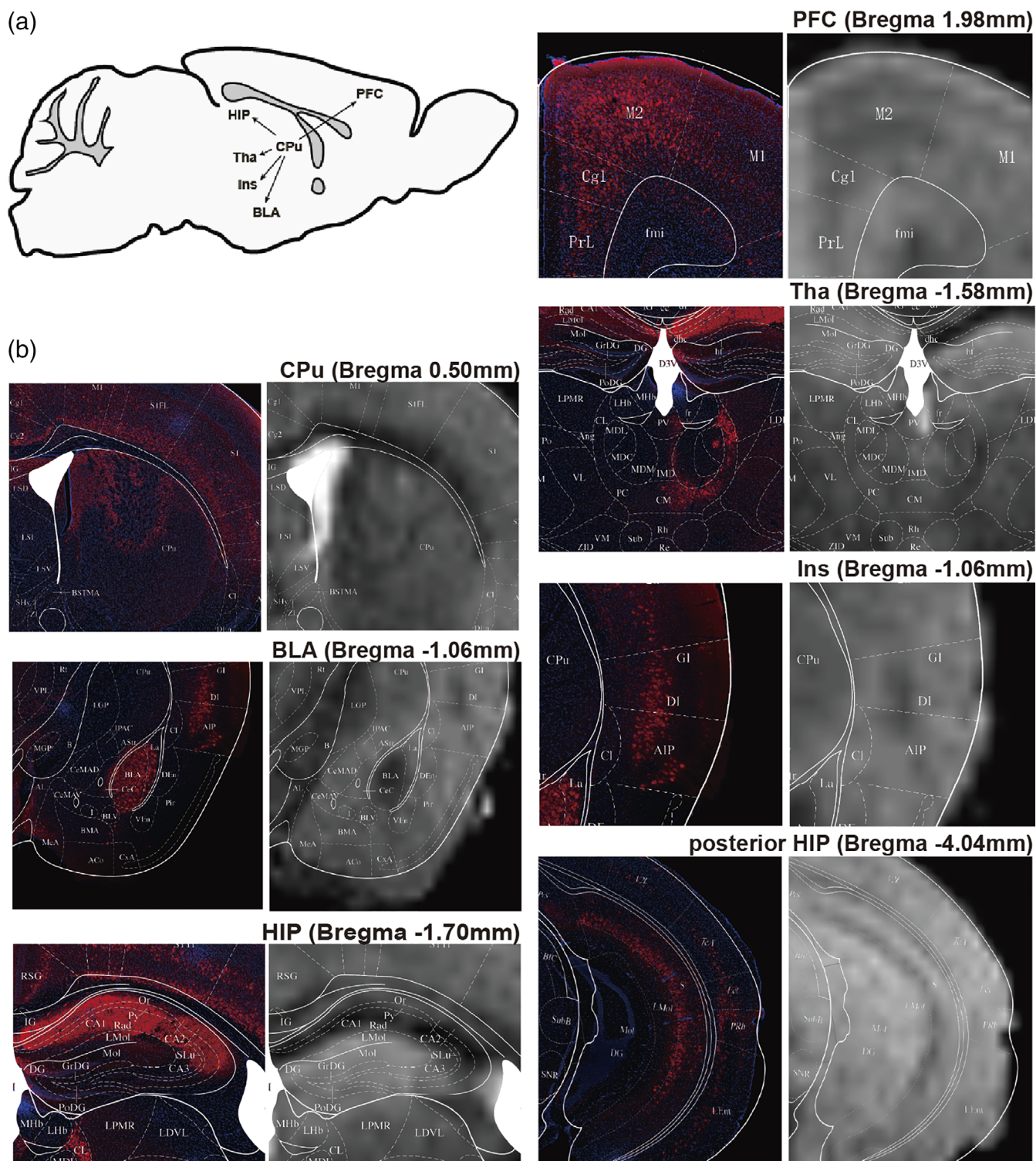


FIGURE 2 Signal comparison of the fluorescence imaging and MRI with brain region segmentation. (a) The sketch map of virus infected regions after the rAAV2-retro injection (shown in fluorescence image). (b) The distribution of Ferritin expression (red) and MRI signal changes (dark) compared at seven regions, CPU, BLA, HIP, PFC, Tha, Ins and post HIP. The mouse brain stereotaxic atlas is overlapped (white) to distinguish the brain structure

overexpression (CSF and SC) were chosen for comparison (Figure S2). One-way ANOVA (LSD post hoc test) was used to test the changes in T2 relaxation time at the eight regions along with the infection days (0d, $N = 14$; 10d, $N = 11$; 30d, $N = 8$; 60d, $N = 5$). As shown in

Figure 6, there was no significant change in the T2 relaxation time detected at CSF or SC where no ferritin was overexpressed during the whole infection period ($p > .05$, marked with same lowercase). Among the other six regions, significant changes were only found at

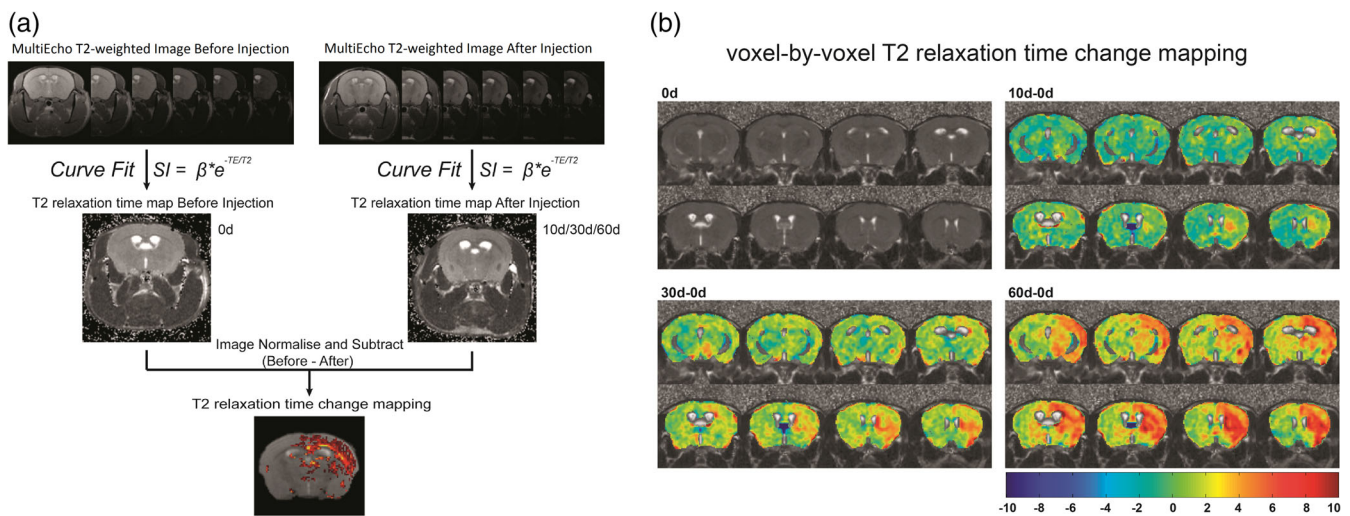


FIGURE 3 The schematic diagram of the processing of multi-Echo T2-weighted images, and the calculation of T2 relaxation time change mapping. (a) The multi-Echo T2-weighted images were firstly transformed to the T2 relaxation time map and then normalized to a template. The normalized T2 relaxation time maps (right) were subtracted with the map of 0d (left) and then screened with a threshold to form a T2 relaxation time change mapping. (b) The voxel-by-voxel T2 relaxation time change mappings in different infection periods

Cpu after 10 days' infection ($p < .05$, marked with different lower-case). When enough time was given for virus infection and ferritin expression, all six regions that ferritin overexpressed showed significant changes after 30 days' infection compared to 0 days' infection. More significant differences could be found in those regions after 60 days' infection time compared to 0 days' or 30 days'.

3 | DISCUSSION

Fluorescence imaging is one of the most commonly used method to visualize results of virus-based neural circuit tracing. However, the depth of fluorescence imaging is always limited by the light transmittance of animal tissues. Although much effort has been made to improve the detection depth of animal fluorescence imaging, it is difficult to show the labeled regions in living animals with a whole-brain view (Cook & Griffin, 2003; Frangioni, 2003; Helmchen & Denk, 2005; Zhu et al., 2020). Herein, the retrograde virus vector AAV that express MRI contrast protein (ferritin) was used to illustrate the neural network in living animals. By injecting the virus into the CPU, we observed a network that directly connected to the CPU using *in vivo* MRI during three different periods after the virus injection. Moreover, the network was confirmed by the fluorescence imaging method. This method could be a powerful approach for exploring the neural circuits *in vivo*.

3.1 | Resolution and SNR of MRI in dissecting neural circuits

Although MRI has the advantages of noninvasive and large imaging scale, the resolution and signal-to-noise ratio are much lower than fluorescence imaging. For fluorescence imaging, the resolution could

reach $0.2 \mu\text{m}$, and there is little interference in the background. Since the diameter of neurons is usually $\sim 5 \mu\text{m}$, the fluorescence imaging can easily distinguish the neuron cells (Cunnane et al., 2019). When using MRI, it is hard to distinguish an individual neuron, due to limited resolution and SNR. However, the resolutions and SNR of MRI are sufficient to distinguish the brain regions for neuronal network detection. In the current study, the distributions of ferritin were always aggregated with significant boundaries, where the T2-weighted images could be utilized to distinguish the change in MRI contrast, such as BLA, Ins and HIP (Figure 2). For the regions of PFC, CPU and Tha, it was not easy to distinguish the ferritin expressed regions from the T2-weighted images, due to the dispersive distribution of ferritin and the low signal intensity of the background. For these regions, the ROIs based statistics analysis of signal intensity and the changes in T2 relaxation time were capable of illustrating the MRI contrast effect caused by ferritin expression. There were also some regions with lower fluorescent signals where the ferritin expression was weak and sparse. For these regions, it was very difficult to distinguish the change in T2-weighted MRI signal intensity. This was probably caused by the low SNR and resolution of MRI, as the weak and sparse ferritin expressions were not sufficient enough to generate the detectable MRI contrast.

3.2 | MRI signals at different infection times

In these experiments, ferritin was overexpressed in a CPU related network through a AAV2-retro virus vector, and three time points (10d, 30d, 60d) were selected to evaluate the ferritin expression and MRI signal. Different ferritin expressions and MRI signals were found at the three time points, and the characteristics of rAAV vector could be the main reason for the differences. The expression of AAV-carrying

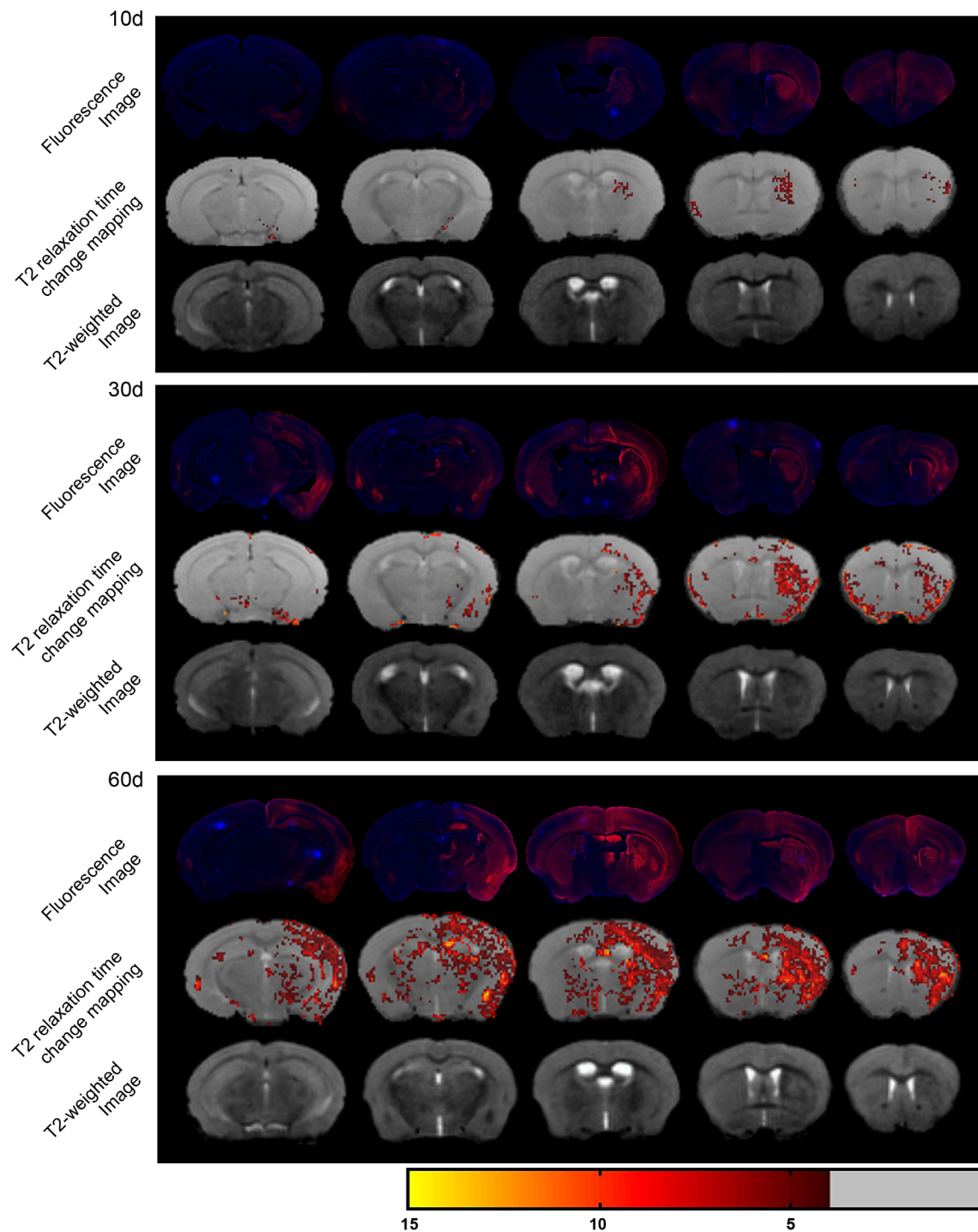


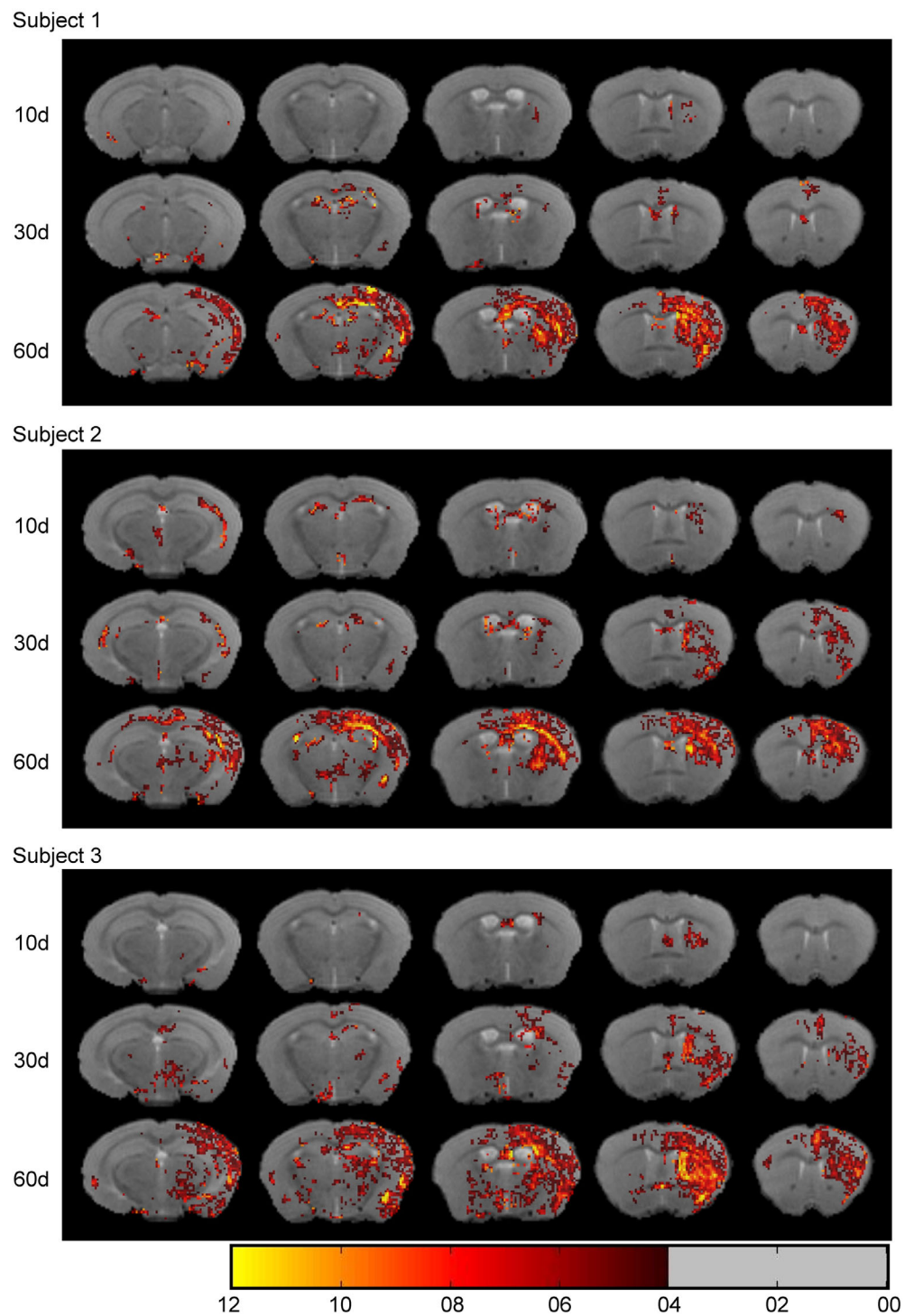
FIGURE 4 The comparison of fluorescence image, T2 relaxation change mapping and T2-weighted image on a different infection day. Three time points after injection are shown (10d, 30d, 60d). Fluorescence images (top) are displayed to show the location and expression quantity of Ferritin at different time points. Corresponding images of the T2 relaxation time change mapping (middle) and the T2-weighted images (bottom) are displayed for comparison. The voxels in T2 relaxation time change mappings are shown with pseudo color (red-yellow) when the value is between 4 ms and 15 ms. MRI and fluorescent images shown here were from three individual mice with different infection time, as the animals were sacrificed for fluorescence imaging

genes usually increases over time and reaches a plateau within 3–12 weeks (Tenenbaum et al., 2004) and most of the AAV2-retro labeled results are obtained within 3–8 weeks as reported. Three weeks (Itoga et al., 2019) and 4 weeks (Itoga et al., 2019) are the most commonly used waiting time for AAV2-retro expression and it is

reported that more labeled information can be obtained using 8 weeks waiting time rather than 4 weeks (Cunnane et al., 2019).

Comparing ferritin expression and MRI signals, incomplete synchronization was detected between ferritin expression and MRI signal changes, especially in the early stage of the virus infection. The

FIGURE 5 The longitudinal study of the rAAV2-retro-CAG-Ferritin infection at three different time points (10d, 30d, 60d) using in vivo MRI. The change in T2 relaxation times before versus after virus injection are used to represent the infected regions of the virus at three time points. The voxels in T2 relaxation time change mappings are shown with pseudo color (red-yellow) when the value is between 4 ms and 12 ms



incomplete synchronization probably results from the characteristics of ferritin. Ferritin itself is not an MRI contrast agent and it influences the MRI signal by recruiting iron ions. There are several parameters influenced by the recruiting iron ions: the quantity of ferritin expressed in the infected region, the distribution of ferritin in cells, the iron enrichment in the intracellular environment, the supplement rate of iron ions and the degradation rate of ferritin. These differences could be the source of the incomplete synchronization between ferritin expression and MRI signals at 10 days and 30 days after the injection. Moreover, the difference between these two signals became smaller when the infection time

reached 60 days, as enough time was given to enrich the iron ions. Further work is needed to shorten the time delay between ferritin expression and MRI contrast generation, such as supplementing iron ions.

3.3 | Relationship between ferritin expression and MRI contrast

Although ferritin is reported to recruit iron ions and influence the MRI signals, there were many factors that influence the MRI signal

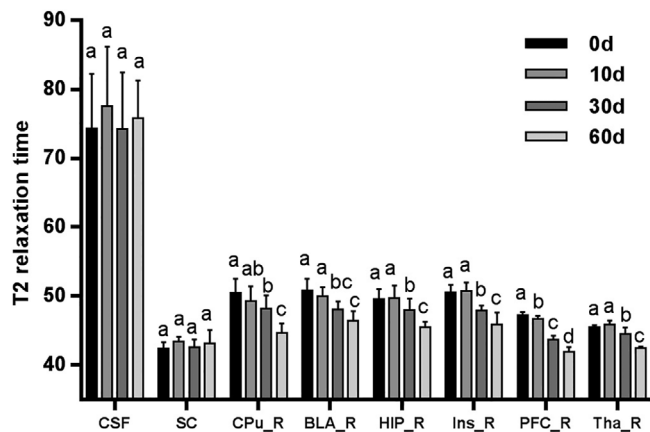


FIGURE 6 Statistics analysis of T2 relaxation times at different time points after rAAV2-retro-CAG-ferritin injection (0d, 10d, 30d, 60d). The T2 relaxation times of six ferritin expressed regions (CPu_R, BLA_R, HIP_R, Ins_R, PFC_R and Tha_R) and two negative control regions without ferritin expressed (CSF and SC) were extracted for comparison. Significant changes among the four time points were calculated using one-way ANOVA with LSD post hoc test, and significant differences between each time point are illustrated with lowercase letters a, b, c, d (a different letter represented $p < .05$ and the same letter represented $p > .05$)

changes. Ferritin is an autologous protein which is involved in inflammation reaction (Namaste et al., 2017), the infection of AAV could hypothetically lead to regional inflammation which could also cause overexpression of ferritin (Vande Velde et al., 2011). Therefore, the expression of ferritin in the infection of rAAV2-retro-CAG-EGFP was also investigated, and no obvious ferritin expression was found (Figure S4). Furthermore, Prussian Blue staining was also utilized to verify the accumulation of Fe^{3+} . The blue complexes were found at the regions where ferritin was overexpressed (Figure S5). Thus, the change in MRI contrast mediated by infection of rAAV2-retro-CAG-Ferritin might have been caused by ferritin overexpression and Fe^{3+} accumulation, rather than inflammation.

Degradation of ferritin could hypothetically cause ferroptosis (Xie et al., 2016), leading to cell death when a mass of unbound iron ions are released to the cell. However, overexpression of ferritin can result in an iron-deficiency intracellular environment (Naumova & Vande Velde, 2018), which could lead to the suppression of ferroptosis (Hou et al., 2016). Prior studies also demonstrated that there is no obvious influence on cells when ferritin is overexpressed (Iordanova & Ahrens, 2012; Iordanova, Goins, Clawson, Hitchens, & Ahrens, 2013). Other than ferroptosis, changes in iron balance of the surrounding tissue around the regions with ferritin overexpression are another potential concern. While this may be a concern for short time periods, iron deficiency could be rebalanced by the blood supply for long time tracing work (more than 10 days). Besides, the expression of apoptosis and inflammation marker, caspase-3 and Iba1, were tested, and no noticeable abnormalities were found in regions BLA, HIP and PFC, where ferritin was overexpressed (Figure 7).

3.4 | Perspective and limitations

Using the ferritin encoding virus, we observed the structural neural network in living mice for a long period after the virus injection. However, the entire neural network was presented in MRI images 60 days after the virus injection. At earlier time points only part of the network was displayed. Our future work could focus on shortening the latency time between the virus injection and MRI detection. Although the ferritin used in our experiment is already an MRI contrast enhanced version (Iordanova, Robison, & Ahrens, 2010), it is possible to make further improvements on the ferritin protein structure for better MRI contrast effect. Besides, exogenous iron ions supplements could be a possible method for providing better MRI contrast effect in shorter latency time (Vande Velde et al., 2011). In addition, the ferritin-encoding virus and in vivo MRI could be used to noninvasively investigate the expression levels of functional elements, such as optogenetic (e.g., ChR2) or chemogenetic (e.g., hM3Dq or hM4Di) proteins. MRI imaging allows for longitudinal observation of virus spread and expression levels of exogenous genes, which can guide further manipulation or operation. This new technique will especially benefit researches on costful non-human primates or big laboratory animals.

4 | MATERIALS AND METHODS

4.1 | Animal preparation

All animals involved in this study were treated in accordance with protocols approved by the Animal Ethics Committee at the Wuhan Institute of Physics and Mathematics, Chinese Academy of Sciences (approval number APM20016A). Male C57BL/6J mice (6–8 weeks old) were purchased from Hunan SJA Laboratory Animal Co., Ltd (Hunan, China) and allowed to acclimate 3 days before the experiment. All the animals were raised under 12 hr/12 hr light–dark cycle room with appropriate temperature, food and water were available ad libitum.

4.2 | Construction of virus

The rAAV2-retro-CAG-Ferritin and the rAAV2-retro-CAG-EGFP virus vector were packaged by a commercial company (BrainVTA, Wuhan, China). This virus will infect neurons in a network in a retrograde manner, moving from axon to soma. Briefly, the plasmids carrying exogenous genes and AAV2-retro packaging components were cotransfected into 293T cells. After 3 days' cultivation, the AAV virions were collected and purified to a titer of $5\text{--}10 \times 10^{12}$ vg/mL. In particular, the ferritin gene used in this experiment was a chimeric ferritin gene (L*H) which comes from the *Mus musculus* ferritin light chain and heavy chain (Gift from Prof. Xiaoming Li's lab in Zhejiang University).

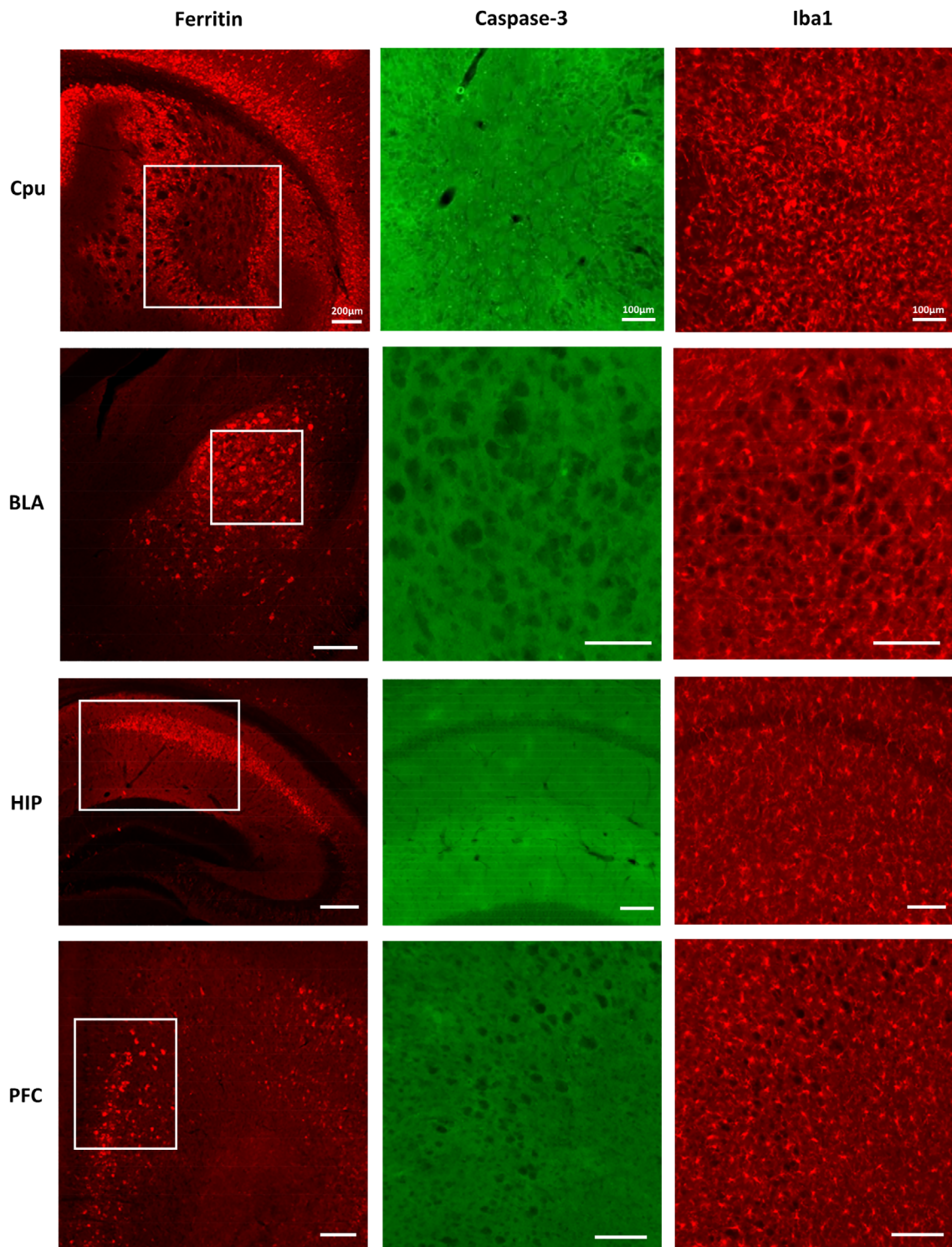


FIGURE 7 The expression of caspase-3 and Iba1 was investigated at the regions that ferritin was overexpressed (red, left). For caspase-3 staining (green, middle), obvious caspase-3 expression can only be observed at the injection site (CPu), and no signal was found at the other three regions (BLA, HIP, and PFC). For Iba1 staining (red, right), no abnormality was observed in the morphology and distribution of microglia

4.3 | Stereotaxic injection

Male C57BL/6J mice were anesthetized with 1.0% pentobarbital sodium (50 mg/kg) and fixed in a stereotaxic injection system (RWD, ShenZhen, China). The skull of each mouse was exposed after being

locally anesthetized with lidocaine lincomycin gel (Xinya, Shanghai, China) and smeared with erythromycin eye ointment to prevent drying. A small hole about 1 mm in diameter was drilled in the skull to allow accessing the glass micropipette. The glass micropipette was stereotaxically injected into the CPu (Figure 8, Caudate Putamen:

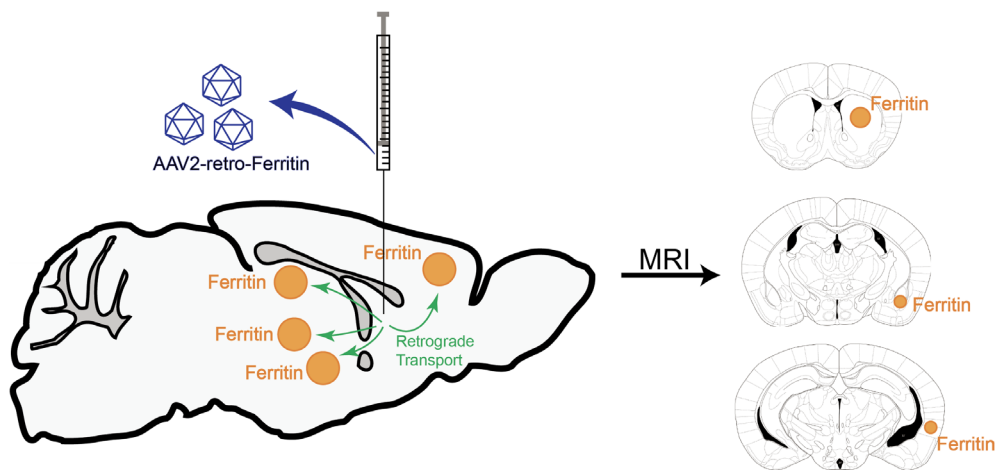


FIGURE 8 Illustration of the schedule of the experiment

0.51 mm anterior to Bregma, 2 mm lateral from midline, 3.3 mm depth relative to Bregma) based on the stereotaxic coordinates of the mouse brain atlas (Paxinos and Franklin). Then, the virus suspension (2.8 μL) with titration of $5\text{--}10 \times 10^{12}$ vg/mL was infused into the CPU at a rate of 0.14 $\mu\text{L}/\text{min}$. After the injection, the micropipette was kept at the injection site for 10 min to prevent reflux and then it was slowly withdrawn. The head skin was surgical sutured after treatment with lidocaine lincomycin gel. At the end of the experiment, the animal was recovered from anesthesia on the heating pad and returned to its home cage.

4.4 | MRI scanning

The *in vivo* MRI experiment was performed using a 7.0 Tesla Biospec small animal magnetic resonance imaging system (Bruker, Ettlingen, Germany). The animals were initially anesthetized with 4.0–5.0% isoflurane (RWD, Shenzhen, China) for induction and 1.0–1.5% for maintenance with a mixture of 30% O_2 and 70% N_2 . The body temperature of animals was maintained with a thermostatic water cycle system under the animal bed. The breathing rate of the animal was monitored and maintained at 60 ± 15 breaths/min to achieve the state of deep anesthesia. In addition, two ear bars and a tooth bar were used to minimize motion effect of MRI data acquisition. A 20 cm birdcage coil was used for transmission, combined with a 20 mm surface coil for receiving (Bruker, Ettlingen, Germany). Multi-echo T2-weighted anatomical images were obtained using an MSME sequence (TR = 3,000 ms; effective TEs = 11, 22, 33, 44, 55, 66 ms; number of averages = 6; FOV = 17.5×17.5 mm²; slice thickness = 0.5 mm; spatial resolution, 0.137 mm \times 0.137 mm). The T2 relaxation time maps were obtained by processing the MSME image using Paravision 5.0 software (Bruker, Germany).

The expression of the rAAV2 in living animals can last for more than 2 months and its expression can reach a maximal level after 30 days (Cunnane et al., 2019). Thus, MRI scans were performed at four time points to study the longitudinal effects of the virus infection. The time points were: the day before the virus injection (0d, $n = 14$), 10 days (10d, $n = 11$), 30 days (30d, $n = 8$) and 60 days after

injection (60d, $n = 5$), respectively. The number of animals was reduced by 3 in each succeeding group as 3 animals were euthanized for the fluorescence study at each time point.

4.5 | Fluorescence imaging and immunohistochemistry

Virus-infected mice were anesthetized with 1.0% pentobarbital sodium (50 mg/kg) and cardiac perfusion was applied with 0.9% saline followed by 4% paraformaldehyde solution. The brain was extracted and dehydrated with 30% (wt/vol) sucrose solution. After that, the dehydrated brain was sectioned into 40 μm slices using freezing microtome (Leica, German) and one of twelve slices were selected for fluorescence imaging (approach to the MRI slice thickness 0.5 mm).

For the imaging of EGFP, the fluorescence imaging was directly performed. For the imaging of ferritin, caspase3, Iba1 or cell nucleus, immunohistochemistry staining was performed before the fluorescence imaging. For immunohistochemistry, the slices were first rinsed with PBS and then blocked with blocking solution buffer (PBS + 0.3% TritonX-100 + 10% goat serum, 37°C, 1 hr). For ferritin staining, the rabbit anti-ferritin light chain antibody (Abcam, ab69090, UK) and Cy3-labeled goat anti-rabbit secondary antibody were utilized. For caspase3 staining, the rabbit anti-caspase3 antibody (Cell Signaling Technology, #9661) and 488-labeled goat anti-rabbit IgG were used. For Iba1 staining, the goat anti-Iba1 antibody (Abcam, ab5) and Cy3-labeled donkey anti-goat antibody were utilized. For cell nucleus staining, the fluorescent dye DAPI was used.

For fluorescence imaging, the brain slices were transferred to microslide and scanned with an Olympus VS120 virtual microscopy slide scanning system (Olympus, Japan). For the filters, Leica U-MRFPHQ fluorescence mirror unit was used for the red fluorescence imaging, which included a 535–555 nm excitation filter, a 575–625 nm emission filter and a 565 nm dichromatic mirror; Leica U-MWIBA3 fluorescence mirror unit was used for green fluorescence imaging, which included a 460–495 nm excitation filter, a 510–550 nm emission filter and a 505 nm dichromatic mirror.

Furthermore, the Perls' Prussian Blue staining method was utilized to verify the accumulation of iron ions. It was performed following a previous study (Kim, Cho, Choi, Woo, & Moon, 2010) with a commercial staining kit (Solarbio, G1422, Beijing, China).

4.6 | Data analysis

The T2-weighted images and T2 relaxation time maps were transformed to NIFTI format using Bru2anz (Bruker, Germany). MRI images were normalized to a homemade mouse MRI template using spm12 (www.fil.ion.ucl.ac.uk). The heavily T2-weighted images (TE/TR = 55 ms/3000 ms) were used to show the MRI signal change in ferritin expressed regions (Figure 8).

For comparison between MRI images and fluorescence images, similar brain slices were chosen based on structural features and the slice position. The anterior commissure was used for feature recognition and the slice with the same axial distance from the anterior commissure was used for these comparisons. The MRI images and fluorescence images were matched with the mouse brain atlas.

For calculating the variation within T2 relaxation times, all the T2 relaxation time maps were firstly nonlinear transformed to a homemade mouse brain template with spm old-normalize. The T2 relaxation times change mapping was obtained by comparing the T2 relaxation time map to the map from the same animal before injection (Od) (Figure 3). The T2 relaxation time changes higher than 15 ms or lower than 4 ms were considered as outliers and deleted.

To quantitatively describe changes in T2 relaxation times, all the MRI images were normalized to a publicly available mouse brain template TMBTA (www.nitrc.org/projects/tmbta_2019) and smoothed. Six regions with ferritin expression (CPu, HIP, BLA, Ins, PFC, Tha) and two regions without ferritin expression (SC, CSF) were chosen as ROIs based on the TMBTA mouse brain atlas (Figure S2). The average T2 relaxation times for the eight ROIs were obtained and these average values were compared using one-way ANOVA. Least significant difference (LSD) was used for post hoc multiple comparisons, with statistical significance at $p < .05$.

5 | CONCLUSION

We developed a novel neural network tracing method using a combination of in vivo MRI and virus tracing techniques. It enabled the detection of the neural network in a living animal with a whole-brain view. Besides, we measured the virus infection progress over a period of time in the same animal. This technology provides a totally different perspective for our understanding of the neural network. It may lead to a different explanation of the brain network when combining the results of in vivo virus tracing and in vivo detection technologies. The technology may also benefit the neural circuit tracing in animals with larger-size brains, of which the whole-brain fluorescence imaging is tremendous amount of work, but easy when using MRI.

ACKNOWLEDGMENTS

This work was supported by grants from the National Natural Science Foundation of China (31970973, 31771193, 21921004), National Natural Science Foundation (NSF) of Hubei Province (2020CFA059), the Strategic Priority Research Program of the Chinese Academy of Sciences (XDB32030200), the Open Project Program of Wuhan National Laboratory for Optoelectronics (2019WNLOKF022) and the Youth Innovation Promotion Association of Chinese Academy of Sciences (Y6Y0021004). Key-Area Research and Development Program of Guangdong Province (2018B030331001).

CONFLICT OF INTEREST

There are no financial conflicts of interest to disclose.

AUTHOR CONTRIBUTIONS

Fuqiang Xu, Jie Wang, Ning Zheng, and Aoling Cai designed the research. Peng Su, Kunzhang Lin, and LingQiang Zhu gave advice on the research. Ning Zheng, Aoling Cai, and Yang Wu performed experiments. Aoling Cai, Ning Zheng, Binbin Nie, and Jinfeng Wu analyzed data. Aoling Cai, Jie Wang, Garth J. Thompson, Ning Zheng, and Anne Manyande wrote the article.

DATA AVAILABILITY STATEMENT

All data and the implementation code in this article are available upon request from the corresponding author (jie.wang@wipm.ac.cn).

ORCID

Jie Wang  <https://orcid.org/0000-0002-2997-3450>

REFERENCES

- Citraro, R., Russo, E., Ngomba, R. T., Nicoletti, F., Scicchitano, F., Whalley, B. J., ... De Sarro, G. (2013). CB1 agonists, locally applied to the cortico-thalamic circuit of rats with genetic absence epilepsy, reduce epileptic manifestations. *Epilepsy Research*, *106*, 74–82.
- Cook, S. H., & Griffin, D. E. (2003). Luciferase imaging of a neurotropic viral infection in intact animals. *Journal of Virology*, *77*, 5333–5338.
- Cunnane, K., Alvarado, A., Gwak, Y., Peters, C., Romero-Sandoval, E., Martin, T., & Eisenach, J. (2019). Studying pain neural circuits with viral vector rAAV2-retro in the brain. *The Journal of Pain*, *20*(4), S36.
- Frangioni, J. V. (2003). In vivo near-infrared fluorescence imaging. *Current Opinion in Chemical Biology*, *7*, 626–634.
- Grandjean, J., Canella, C., Anckaerts, C., Ayranci, G., Bougacha, S., Bienert, T., ... Gozzi, A. (2020). Common functional networks in the mouse brain revealed by multi-centre resting-state fMRI analysis. *NeuroImage*, *205*, 116278.
- Helmchen, F., & Denk, W. (2005). Deep tissue two-photon microscopy. *Nature Methods*, *2*, 932–940.
- Hong, G., Diao, S., Chang, J., Antaris, A. L., Chen, C., Zhang, B., ... Dai, H. (2014). Through-skull fluorescence imaging of the brain in a new near-infrared window. *Nature Photonics*, *8*, 723–730.
- Hong, G. S., Antaris, A. L., & Dai, H. J. (2017). Near-infrared fluorophores for biomedical imaging. *Nature Biomedical Engineering*, *1*(1), 1–22.
- Hou, W., Xie, Y., Song, X., Sun, X., Lotze, M. T., Zeh, H. J., 3rd, ... Tang, D. (2016). Autophagy promotes ferroptosis by degradation of ferritin. *Autophagy*, *12*, 1425–1428.
- Iordanova, B., & Ahrens, E. T. (2012). In vivo magnetic resonance imaging of ferritin-based reporter visualizes native neuroblast migration. *NeuroImage*, *59*, 1004–1012.

- Iordanova, B., Goins, W. F., Clawson, D. S., Hitchens, T. K., & Ahrens, E. T. (2013). Quantification of HSV-1-mediated expression of the ferritin MRI reporter in the mouse brain. *Gene Therapy*, *20*, 589–596.
- Iordanova, B., Robison, C. S., & Ahrens, E. T. (2010). Design and characterization of a chimeric ferritin with enhanced iron loading and transverse NMR relaxation rate. *Journal of Biological Inorganic Chemistry*, *15*, 957–965.
- Itoga, C. A., Chen, Y., Fateri, C., Echeverry, P. A., Lai, J. M., Delgado, J., ... Xu, X. (2019). New viral-genetic mapping uncovers an enrichment of corticotropin-releasing hormone-expressing neuronal inputs to the nucleus accumbens from stress-related brain regions. *The Journal of Comparative Neurology*, *527*, 2474–2487.
- Kaplitt, M. G., Feigin, A., Tang, C., Fitzsimons, H. L., Mattis, P., Lawlor, P. A., ... During, M. J. (2007). Safety and tolerability of gene therapy with an adeno-associated virus (AAV) borne GAD gene for Parkinson's disease: An open label, phase I trial. *Lancet*, *369*, 2097–2105.
- Kim, H. S., Cho, H. R., Choi, S. H., Woo, J. S., & Moon, W. K. (2010). In vivo imaging of tumor transduced with bimodal lentiviral vector encoding human ferritin and green fluorescent protein on a 1.5T clinical magnetic resonance scanner. *Cancer Research*, *70*, 7315–7324.
- Li, X. F., Li, X. D., Deng, C. L., Dong, H. L., Zhang, Q. Y., Ye, Q., ... Qin, C. F. (2017). Visualization of a neurotropic flavivirus infection in mouse reveals unique viscerotropism controlled by host type I interferon signaling. *Theranostics*, *7*, 912–925.
- Namaste, S. M., Rohner, F., Huang, J., Bhushan, N. L., Flores-Ayala, R., Kupka, R., ... Suchdev, P. S. (2017). Adjusting ferritin concentrations for inflammation: Biomarkers reflecting inflammation and nutritional determinants of anemia (BRINDA) project. *The American Journal of Clinical Nutrition*, *106*, 359S–371S.
- Nassi, J. J., Cepko, C. L., Born, R. T., & Beier, K. T. (2015). Neuroanatomy goes viral! *Frontiers in Neuroanatomy*, *9*, 80.
- Naumova, A. V., & Vande Velde, G. (2018). Genetically encoded iron-associated proteins as MRI reporters for molecular and cellular imaging. *WIREs Nanomedicine and Nanobiotechnology*, *10*(2), e1482.
- Pagani, M., Damiano, M., Galbusera, A., Tsaftaris, S. A., & Gozzi, A. (2016). Semi-automated registration-based anatomical labelling, voxel based morphometry and cortical thickness mapping of the mouse brain. *Journal of Neuroscience Methods*, *267*, 62–73.
- Rao, X., & Wang, J. (2020). Neuronal network dissection with neurotropic virus tracing. *Neuroscience Bulletin*, *36*, 199–201.
- Rozov, A., Jerecic, J., Sakmann, B., & Burnashev, N. (2001). AMPA receptor channels with long-lasting desensitization in bipolar interneurons contribute to synaptic depression in a novel feedback circuit in layer 2/3 of rat neocortex. *The Journal of Neuroscience*, *21*, 8062–8071.
- Tenenbaum, L., Chtarto, A., Lehtonen, E., Velu, T., Brotchi, J., & Levivier, M. (2004). Recombinant AAV-mediated gene delivery to the central nervous system. *The Journal of Gene Medicine*, *6*(Suppl. 1), S212–S222.
- Tervo, D. G., Hwang, B. Y., Viswanathan, S., Gaj, T., Lavzin, M., Ritola, K. D., ... Karpova, A. Y. (2016). A designer AAV variant permits efficient retrograde access to projection neurons. *Neuron*, *92*, 372–382.
- Ugolini, G. (2010). Advances in viral transneuronal tracing. *Journal of Neuroscience Methods*, *194*, 2–20.
- Ullmann, J. F., Watson, C., Janke, A. L., Kurniawan, N. D., & Reutens, D. C. (2013). A segmentation protocol and MRI atlas of the C57BL/6J mouse neocortex. *NeuroImage*, *78*, 196–203.
- Van Leemput, K., Bakkour, A., Benner, T., Wiggins, G., Wald, L. L., Augustinack, J., ... Fischl, B. (2009). Automated segmentation of hippocampal subfields from ultra-high resolution in vivo MRI. *Hippocampus*, *19*, 549–557.
- Vande Velde, G., Rangarajan, J. R., Toelen, J., Dresselaers, T., Ibrahim, A., Krylychkina, O., ... Baekelandt, V. (2011). Evaluation of the specificity and sensitivity of ferritin as an MRI reporter gene in the mouse brain using lentiviral and adeno-associated viral vectors. *Gene Therapy*, *18*, 594–605.
- Wei, P., Liu, N., Zhang, Z., Liu, X., Tang, Y., He, X., ... Wang, L. (2015). Processing of visually evoked innate fear by a non-canonical thalamic pathway. *Nature Communications*, *6*, 6756.
- Wei, Y. C., Wang, S. R., Jiao, Z. L., Zhang, W., Lin, J. K., Li, X. Y., ... Xu, X. H. (2018). Medial preoptic area in mice is capable of mediating sexually dimorphic behaviors regardless of gender. *Nature Communications*, *9*, 279.
- Wu, E. X., Wong, K. K., Andrassy, M., & Tang, H. (2003). High-resolution in vivo CBV mapping with MRI in wild-type mice. *Magnetic Resonance in Medicine*, *49*, 765–770.
- Wu, Q., Ono, K., Suzuki, H., Eguchi, M., Yamaguchi, S., & Sawada, M. (2018). Visualization of Arc promoter-driven neuronal activity by magnetic resonance imaging. *Neuroscience Letters*, *666*, 92–97.
- Xie, Y., Hou, W., Song, X., Yu, Y., Huang, J., Sun, X., ... Tang, D. (2016). Ferroptosis: Process and function. *Cell Death and Differentiation*, *23*, 369–379.
- Zhang, Z., Liu, Q., Wen, P., Zhang, J., Rao, X., Zhou, Z., ... Xu, F. (2017). Activation of the dopaminergic pathway from VTA to the medial olfactory tubercle generates odor-preference and reward. *eLife*, *6*, e25423.
- Zheng, N., Su, P., Liu, Y., Wang, H., Nie, B., Fang, X., ... Xu, F. (2019). Detection of neural connections with ex vivo MRI using a ferritin-encoding trans-synaptic virus. *NeuroImage*, *197*, 133–142.
- Zheng, N., Wang, Z. Z., Wang, S. W., Yang, F. J., Zhu, X. T., Lu, C., ... Xu, F. Q. (2020). Co-localization of two-color rAAV2-retro confirms the dispersion characteristics of efferent projections of mitral cells in mouse accessory olfactory bulb. *Zoological Research*, *41*, 148–156.
- Zhu, J., Yu, T., Li, Y., Xu, J., Qi, Y., Yao, Y., ... Zhu, D. (2020). MACS: Rapid aqueous clearing system for 3D mapping of intact organs. *Advanced Science (Weinheim)*, *7*, 1903185.

SUPPORTING INFORMATION

Additional supporting information may be found online in the Supporting Information section at the end of this article.

How to cite this article: Cai, A., Zheng, N., Thompson, G. J., Wu, Y., Nie, B., Lin, K., Su, P., Wu, J., Manyande, A., Zhu, L. Q., Wang, J., & Xu, F. (2021). Longitudinal neural connection detection using a ferritin-encoding adeno-associated virus vector and in vivo MRI method. *Human Brain Mapping*, *42*(15), 5010–5022. <https://doi.org/10.1002/hbm.25596>